Severe combined immunodeficiency in stimulator of interferon genes (STING) V154M/wild-type mice

Delphine Bouis, Peggy Kirstetter, Florent Arbogast, Delphine Lamon, Virginia Delgado, Sophie Jung, Claudine Ebel, Hugues Jacobs, Anne-Marie Knapp, Nadia Jeremiah, et al.

Severe combined immunodeficiency in Sting V154M/WT mice

Delphine Bouis, PharmD, MSc,[1] Peggy Kirstetter, PhD,[2,3,4] Florent Arbogast, MSc,[1,5] Delphine Lamon, TA,[1] Virginia Delgado, PhD,[1] Sophie Jung, DDS, PhD,[1,6] Claudine Ebel, GE,[2,3,4] Hugues Jacobs, PhD,[2,3,4,7,8] Anne-Marie Knapp, GE,[1,9] Nadia Jeremiah, PhD,[10] Alexandre Belot, MD, PhD,[11,12] Thierry Martin, MD, PhD,[1,9,13] Yanick J Crow, MD, PhD,[14,15,16] Isabelle André-Schmutz, PhD,[15,17] Anne-Sophie Korganow, MD, PhD,[1,9,13] Frédéric Rieux-Laucat, PhD,[15,18] & Pauline Soulas-Sprauel, PharmD, PhD,[1,13,19*]

[1] CNRS UPR 3572 "Immunopathology and Therapeutic Chemistry"/Laboratory of Excellence Medalis, Institute of Molecular and Cellular Biology (IBMC), Strasbourg, France.
[2] Institut de Génétique et de Biologie Moléculaire et Cellulaire (IGBMC), Illkirch, France.
[3] Institut National de la Santé et de la Recherche Médicale (INSERM), U964, Illkirch, France.
[4] Université de Strasbourg, 1 rue Laurent Fries, 67404 Illkirch, France.
[5] UFR Sciences de la Vie, Université de Strasbourg, Strabsourg, France.
[6] Hôpitaux Universitaires de Strasbourg, Pôle de Médecine et de Chirurgie Bucco-dentaires, Centre de référence des maladies rares orales et dentaires (O'Rares) et Université de Strasbourg, Faculté de Chirurgie Dentaire, Strasbourg, France.
[7] Centre National de Recherche Scientifique (CNRS), UMR7104, Illkirch, France.
[8] CELPHEDIA, PHENOMIN, Institut Clinique de la Souris (ICS), 1 rue Laurent Fries, F-67404 Illkirch-Graffenstaden, France.
[9] UFR Médecine, Université de Strasbourg, Strasbourg, France.
[10] Immunity and Cancer Department, Institut Curie, PSL Research University, INSERM U932, 75005 Paris, France.
[11] Service de Néphrologie, Rhumatologie, Dermatologie pédiatriques, Centre de référence RAISE, HFME, Hospices Civils de Lyon, Lyon, France.
[12] INSERM UMR 1111, Université de Lyon, Lyon, France.
[13] Department of Clinical Immunology and Internal Medicine, National Reference Center for Autoimmune Diseases, Hôpitaux Universitaires de Strasbourg, Strasbourg, France.
[14] INSERM UMR 1163, Laboratory of Neurogenetics and Neuroinflammation, F-75015 Paris, France
[15] Paris Descartes – Sorbonne Paris Cité University, Imagine Institute, F-75015 Paris, France.
[16] Division of Evolution and Genomic Sciences, School of Biological Sciences, Faculty of Biology, Medicine and Health, University of Manchester, Manchester Academic Health

Science Centre, Manchester, UK.
[17] Laboratory of Human Lymphohematopoiesis, INSERM UMR 1163, F-75015 Paris, France.
[18] Laboratory of Immunogenetics of Pediatric autoimmune Diseases, INSERM UMR 1163, F-75015 Paris, France.
[19] UFR Sciences pharmaceutiques, Université de Strasbourg, Illkirch-Graffenstaden, France.

*__Corresponding author:__
Pauline SOULAS-SPRAUEL, PharmD, PhD
CNRS UPR 3572 "Immunopathology and Therapeutic Chemistry"
Institute of Molecular and Cellular Biology (IBMC)
15 rue René Descartes, 67084 Strasbourg Cedex, FRANCE
Phone number: + 33 3 88 41 70 25
Fax: + 33 3 88 61 06 80
E-mail address: pauline.soulas@ibmc-cnrs.unistra.fr

ABSTRACT

BACKGROUND: Autosomal dominant gain-of-function (GOF) mutations in human STING (Stimulator of Interferon Genes) lead to a severe autoinflammatory disease called SAVI (STING Associated Vasculopathy with onset in Infancy), associated with enhanced expression of interferon (IFN) stimulated gene (ISG) transcripts.

OBJECTIVE: The goal of this study was to analyze the phenotype of a new mouse model of Sting hyperactivation, and the role of type I IFN in this system.

METHODS: We generated a knock-in model carrying an amino acid substitution (V154M) in mouse Sting, corresponding to a recurrent mutation seen in human patients with SAVI. Hematopoietic development and tissue histology were analyzed. Lymphocyte activation and proliferation were assessed *in vitro*. Sting V154M/WT mice were crossed to IFNAR (IFNα/β Receptor) knock-out mice in order to evaluate the type I IFN-dependence of the mutant Sting phenotype recorded.

RESULTS: In Sting V154M/WT mice we detected variable expression of inflammatory infiltrates in the lungs and kidneys. These mice showed a marked decrease in survival and developed a severe combined immunodeficiency disease (SCID) affecting B, T and NK cells, with an almost complete lack of antibodies and a significant expansion of monocytes and granulocytes. The blockade in B and T cell development was present from early immature stages in bone marrow and thymus. In addition, *in vitro* experiments revealed an intrinsic proliferative defect of mature T cells. Whilst the V154M/WT mutant demonstrated increased expression of ISGs, the SCID phenotype was not reversed in Sting V154M/WT IFNAR knock-out mice. However, the anti-proliferative defect in T cells was partially rescued by IFNAR deficiency.

CONCLUSIONS: Sting GOF mice developed an IFN-independent SCID phenotype with a T, B and NK cell developmental defect and hypogammaglobulinemia, associated with signs of inflammation in lungs and kidneys. Only the intrinsic proliferative defect of T cells was, partially, IFN-dependent.

KEY MESSAGES

- A Sting V154M/WT murine model demonstrated a severe combined immunodeficiency (SCID) affecting B, T and NK cells, with a significant expansion of monocytes and granulocytes. This SCID phenotype was independent of the type I IFN pathway, despite the observation of a significant upregulation of IFN induced gene transcripts.
- An anti-proliferative effect was noticed in T cells, which was partially IFN-dependent.
- Variable inflammation of lung and kidney was observed.

CAPSULE SUMMARY

Sting V154M/WT mice develop an IFN-independent severe combined immunodeficiency with hypogammaglobulinemia, a partially IFN-dependent T cell proliferation defect, and variable lung and kidney inflammation, providing new clues in the understanding of STING gain-of-function pathophysiology.

KEY WORDS

Severe combined immunodeficiency, STING, V154M, type I interferon

ABBREVIATIONS

BM	Bone marrow
CD	Cluster of Differentiation
cGAMP	cyclic GMP-AMP
CLP	Common lymphoid progenitor
CMP	Common myeloid progenitor
Cxcl10/IP10	Interferon-γ-inducible protein 10
DD	Dimerization domain
DN	Double negative
DP	Double positive
ER	Endoplasmic reticulum
ETP	Early T cell progenitor
GMP	Granulocyte/monocyte progenitor
GOF	Gain-of-function
Ifit1	Interferon-induced protein with tetratricopeptide repeats 1

100	IFN	Interferon
101	IFNAR	Interferon α/β receptor
102	Ig	Immunoglobulin
103	IL	Interleukin
104	ILCs	Innate Lymphoid cells
105	IRF3	Interferon regulatory factor 3
106	Isg15	Interferon stimulated gene 15
107	ISGs	Interferon stimulated genes
108	KO	Knock-out
109	LT-HSC	Long-Term hematopoietic stem cells
110	LNs	Lymph nodes
111	LTα	Lymphotoxin α
112	LTi	Lymphoid Tissue-inducing cells
113	MCP-1	Monocyte chemotactic protein-1
114	MEP	Megakaryocyte/erythroid progenitor
115	MPP	Multipotent progenitor
116	PAMPs	Pathogen associated molecular patterns
117	SAVI	Sting associated vasculopathy with onset in infancy
118	SCID	Severe combined immune deficiency
119	SLE	Systemic lupus erythematosus
120	STAT6	Signal transducer and activator of transcription 6
121	ST-HSC	Short-term hematopoietic stem cells
122	STING	Stimulator of interferon genes
123	TBK1	Tank-binding kinase 1
124	TNFα	Tumor necrosis factor α
125	Tregs	Regulatory T cells
126	WT	Wild-type

INTRODUCTION

Since its identification as an adaptor molecule in the cytosolic DNA-sensing pathway, Stimulator of Interferon Genes (STING) has emerged as a central player in antiviral and antibacterial immunity, autoinflammation and cancer[1-5]. STING is an endoplasmic reticulum (ER)-associated membrane protein, which is expressed in a wide variety of tissues including endothelial, epithelial and hematopoietic cell types[6,7]. Signaling through STING can be induced by cyclic di-GMP, cyclic di-AMP and cyclic GMP–AMP (cGAMP). Such pathogen associated molecular patterns (PAMPs) are recognized by STING, causing its activation and subsequent migration from the ER to perinuclear vesicles where it recruits and activates the TANK-binding kinase 1 (TBK1). STING-TBK1 then induces the phosphorylation, dimerization and nuclear translocation of interferon regulatory factor 3 (IRF3), which drives a type I IFN response[8] and the expression of a set of interferon (IFN)-stimulated genes (ISGs). The STING–TBK1 axis is also known to phosphorylate IkB, resulting in NF-κB release, nuclear translocation and increased NF-κB-dependent gene expression, a pathway implicated in cellular stress, tumor progression, inflammation and immunity[9]. Finally, this axis can also lead to the phosphorylation of Signal transducer and activator of transcription 6 (STAT6), which mediates immune signaling in response to cytokines and to virus infection[10].

STING is therefore an adaptor of DNA sensing, which appears to be critical for the detection of diverse cytosolic cyclic dinucleotides and DNA[11]. Usually confined to the nucleus and mitochondria, in some circumstances abnormal host DNA can be found in the cytoplasm, leading to the development of autoimmune features in mice and humans[12,13]. For this reason, in the homeostatic context, STING-mediated signaling has to be finely regulated, since chronic or constitutive activation, for example due to genetic mutation, might otherwise lead to autoinflammation[14]. Indeed, a number of gain-of-function (GOF) mutations in *TMEM173*, encoding STING, have been described in patients with an autoinflammatory phenotype designated Sting Associated Vasculopathy with onset in Infancy (SAVI)[15,16]. SAVI is considered part of a group of diseases referred to as type I interferonopathies, where type I IFN-induced signaling is considered to play a central role in disease pathology[17,18]. SAVI patients variably demonstrate systemic inflammation, and inflammatory lesions of the skin and lungs. T and NK lymphopenia is a consistent feature, although patients do not present with classical symptoms of immunodeficiency such as severe susceptibility to pathogens. Autoimmunity is also very rare[7,15,16]. Today, the exact molecular mechanisms leading to these various features remain uncertain.

Twenty two patients from 15 families have been reported with heterozygous GOF mutations in *TMEM173* involving amino acids at positions 147, 154, 155 and 166, localized near to (V147L) or within the dimerization domain (DD) (N154S, V155M, G166E) of STING protein [15,16,19-24]. These changes have been suggested to lead to the stabilization of the DD, and thus constitutive activation of STING[15,16]. Three other SAVI patients have been described, carrying distinct mutations (namely C206Y in exon 6; R281Q and R284G in exon 7), located in the cGAMP binding domain (CBD) of STING, also leading to constitutive activation of the protein, thereby implicating a second region of STING important in type I IFN signaling[7].

Here, we generated a new knock-in mouse model with the heterozygous V154M mutation, corresponding to the V155M mutation in humans (the most frequent mutation described so far), in order to better understand the impact of this mutation on the immune system and the role of the type I IFN-pathway in SAVI. These mice developed a SCID phenotype, with a T, B and NK lymphopenia, a strong hypogammaglobulinemia, and an expansion in the myeloid population, which were IFN-dependent. They also developed variable lung and kidney inflammation.

MATERIALS AND METHODS

Generation of Sting V154M$^{+/-}$ knock-in mice

The V154M mutation was introduced in the Tmem173 locus using a standard CRISPR-meditated genome editing procedure (Taconic). In short, after administration of hormones, superovulated C57BL/6NJ females were mated with C57BL/6NJ males. One cell stage fertilized embryos were placed in a drop of M2 medium under mineral oil. A microinjection pipette with an approximate internal diameter of 0.5 micrometers (at the tip) was used to inject the mixed nucleotide preparation containing the Cas9-protein and the specific gRNA (Fig 1, A) into the pronucleus of each embryo. After injection, 35 injected one-cell stage embryos were transferred to one of the oviducts of pseudopregnant NMRI females. Founder animals were identified by PCR of the targeted locus following NcoI digestion. PCR samples per founder were subcloned and multiple clones were analyzed by DNA-sequencing to confirm the presence of the V145M mutation and exclude the presence of additional mutations near the target sequence. One founder animal was then selected for an *in vitro* fertilization procedure to generate G1 heterozygous pups. Predicted potential off-target sites were analyzed in G1 heterozygous animals by targeted sequencing.

Mice

Mice were bred and backcrossed on a C57BL/6N background for 8 generations in specific pathogen free (SPF) conditions at the animal facility of the Molecular and Cellular Biology Institute (IBMC, Strasbourg). Littermate WT mice were always used as controls. As indicated in the Results section for some experiments, Sting V154M/WT and WT littermate control mice were treated the whole time with antibiotic in drinking water (Baytril® 10% oral solution, Enrofloxacin 150µL per 100mL of filtrated and autoclaved water; drinking water changed every week). Sting V154M/WT mice were crossed with IFNAR knock-out mice (provided by CDTA, CNRS, Orléans, France)[25].

Genotyping of Sting V154M$^{+/-}$ mice was assessed by PCR amplification of genomic DNA extracted from tail samples, using the following primers: one forward primer in exon 4 (5'-ATAGCAGTGCTGAGAGCAAGC -3') and one reverse primer in exon 6 (5'-GGGATCTAATGCTCTCTTCTGG -3'). PCR products are then treated for one hour at 37°C with NcoI restriction enzyme (New England Biolabs) in order to distinguish the WT allele (1 band) from the mutated one (3 bands). PCR was performed with initial denaturation (95°C, 5 min) followed by 35 cycles of denaturation (95°C, 30 sec), annealing (61.5°C, 30 sec) and extension (72°C, 1 min). Genotyping of IFNAR KO mice was assessed by PCR amplification with the following combination of primers: Forward 5'-AAGATGTGCTGTTCCCTTCCTCTGCTCTGA -3', Reverse 5'-ATTATTAAAAGAAAAGACGAGGCGAAGTGG -3' and a third one 5'CCTGCGTGCAATCCATCTTG-3'. PCR was performed as follow: 95°C, 3 min and 35 cycles 94°C 15 sec, 62°C 15 seconds and 72°C 30 sec.

All animal experiments were performed with the approval of the ''Direction départementale des services vétérinaires'' (Strasbourg, France) and protocols were approved by the ethics committee (''Comité d'éthique en matière d'Experimentation Animale de Strasbourg'', CREMEAS) under relevant institutional authorization ("Ministère de l'Education Nationale, de l'Enseignement Supérieur et de la Recherche"), authorization number: 2015072907553237 (APAFIS#2387). All control mice used in experiments were littermate controls.

Western Blotting

Cell lysates were prepared from splenic-sorted CD43 negative naive B cells. Proteins were size-fractionated by 4%-20% gradient SDS-PAGE, electrotransferred to a PVDF membrane for 1.5 h at 130V, and immunodetected with rabbit polyclonal anti-mouse Sting antibody (ProteinTech). Sting protein (band of ~40kDa) was detected with a secondary horseradish

peroxidase-conjugated goat anti-rabbit IgG antibody (Jackson ImmunoResearch). Anti-β Actin Ab (Santa Cruz) was used as protein loading control.

Flow cytometry analysis

Analyses of cell phenotype and proliferation rates were performed on splenic, thymic and bone marrow lymphoid populations using a four-color fluorescence cytometer (FACSCalibur™) according to standard protocols. The following antibodies were used: FITC, PE, PerCP or APC anti–mouse IgM, CD19, B220, CD3, CD4, CD8, CD21, CD23, CD44, CD62L, Mac1 (CD11b), Gr1 (Ly6C/G), CD49b, NK1.1 (CD161), CD86, CD25, CD138, FoxP3 (all from BD Biosciences). Propidium iodide (2.5µg/mL, Sigma) or FvD (Fixable viability dye) were used for discrimination of live and dead cells. The following antibodies were used for bone marrow and thymic progenitor analysis : PerCP Cy5.5, APC, Alexa 488, APC-e-Fluor780, BV 421, BV 605, PE, Alexa 700, PE-Cy7, FITC, Cy5, APC-Cy7, PE-CF594, PE-eFluor610 or e-Fluor450 anti-mouse CD11b, CD11c, CD317, Gr1, Lineage, ckit, Sca1, CD48 (from e-Biosciences), Ter119, CD71, , CD127, CD34, CD16/32 (from BD Biosciences) and CD150 (from Biolegend). Lineage staining correspond to the following antibodies: anti-mouse CD3, CD4, CD8, B220, CD11b, CD11c, Gr1, CD49b and Ter119 (Ly76). These analyses were performed using a ten-color fluorescence cytometer (FACS FORTESSA™), according to standard protocols. The following antibodies were used for spleen, bone marrow or thymic proliferation and apoptosis analysis, respectively: FITC anti-BrdU (see **5-bromo-2'-deoxyuridine (BrdU) incorporation**) and FITC annexin V (from BD Biosciences). Data were analyzed with FlowJo software (Treestar®).

5-bromo-2'-deoxyuridine (BrdU) incorporation

BrdU was firstly administered by intraperitoneal injection of 100µL BrdU (1mg/mL; Sigma) 72 hours prior to analysis, and also delivered to mice in their drinking water at a concentration of 0.8 mg/ml. Bone marrow and thymus were collected 72 hours after the BrdU injection. Cells were fixed with Cytofix/Cytoperm buffer (BD Biosciences) and permeabilized with the permeabilization buffer (BD Biosciences). DNA was then denatured with a DNAse solution (100µg/mL, BD Biosciences) in order to improve the accessibility of the incorporated BrdU to the detection antibody. A FITC mouse anti-BrdU antibody was used to detect the incorporated BrdU. Cells were then analyzed by flow cytometry.

Complete Blood Count

Blood (150µL) was collected in EDTA 2% anticoagulant solution (30µL per 100µL of blood). Complete blood counts (WBC, RBC, Hemoglobin dosage) were performed in the Mouse Clinic Institute (ICS, Illkirch, France).

Antibody detection by ELISA

Total IgM, IgG and IgA levels were measured in serum from 3 to 6-month-old mice or in culture supernatant after stimulation. Sera were obtained by blood centrifugation at 6000 rpm for 6 min. Levels of total immunoglobulins were measured as previously described[26]. Absorbance was then read at 492 nm with the Multiskan^{TM} FC photometer (ThermoFisher) and analysed with SkanIt^{TM} microplate reader software. The concentration of total serum Ig was evaluated by comparison with a standard curve using purified mouse IgM, IgG or IgA standards (Sigma, ref. M-5170; Jackson ImmunoResearch, ref. 015000003; BD, ref. 553476).

Cell preparation and culture

In vitro B- and T-cell stimulations were performed in complete RPMI-1640 medium containing L-glutamine (Lonza) supplemented with 10% FCS (Dutscher), 50 mM β-Mercaptoethanol (Gibco) 1% Penicillin/Streptomycin (Gibco), 10 mM HEPES (Lonza), and 1 mM Sodium Pyruvate (Lonza). Splenic naïve (CD43 negative) B cells were purified by negative magnetic selection (mouse CD43 (Ly-48) MicroBeads; MACS Miltenyi Biotech) and splenic T cells with Dynabeads Untouched Mouse T cells kit (Invitrogen), according to the supplier's protocols. B cells were stimulated with either LPS from *Salmonella typhosa* (10 µg/ml, Sigma-Aldrich) or goat anti-IgM alone (10µg/mL, Jackson ImmunoResearch), a combination of anti-CD40 antibody and recombinant murine IL-4 (1µg/mL, 5ng/mL; 5 ng/mL, Sigma), or a combination of anti-IgM and anti-CD40 for 3 or 4 days, depending on the experiment. For T cell stimulation, plates were coated with anti-CD3 (BD Pharmingen, 10µg/mL) 4 hours at 37°C or O/N at 4°C and cells were then stimulated with anti-CD28 (BD Pharmingen, 10µg/mL), for 3 days at 37°C. For proliferation analysis, splenocytes or sorted splenic mature B cells were pre-treated with CFSE dye (carboxyfluorescein diacetate succinimidyl ester) (Sigma), according to standard protocols, before being cultured for 4 days at 37°C. Plasmabast differentiation ($B220^{low}$CD138+ cells) was determined by flow cytometry.

Quantitative real-time RT-PCR analysis

RNA was extracted with RNeasy Kit (Qiagen) and cDNA was obtained with High Capacity Reverse Transcription Kit (Applied Biosystems) using a T100™ Thermal cycler (Biorad). Quantitative real-time PCR was performed on 10 ng of cDNA using Taqman Universal Mastermix (Applied Biosystems) and Assays-on-Demand probes (Applied Biosystems) (*Hprt1*: Mm01318743_m1, *Gapdh*: Mm03302249_g1, *Sting*: Mm01158117_m1, *Isg15*: Mm01705338_s1, *Ifit1*: Mm00515153_m1, *Cxcl10*: Mm00445235_m1, *Ifnα4*: Mm00833969_s1, *Ifnβ1*:Mm00439552_s1). Each sample was amplified in triplicate in a StepOnePlus® real-time PCR system (Applied Biosystems). mRNA levels were calculated with the StepOne v2.1 software (Applied Biosystems), using the comparative cycle threshold method, and normalized to the mean expression of *Hprt1* and *Gapdh* housekeeping genes.

Histological analysis

Histological processing and evaluation was performed in the Mouse Clinic Institute (iCS) on 5 µm thick sections obtained from formalin-fixed paraffin embedded tissues (bones have been decalcified in rapid decalcifier for 2 hours [DC3, *VWR Chemicals*]). All tissues were stained with hematoxylin and eosin (H&E). Lungs and kidneys were also stained using Masson's trichrome method to demonstrate possible fibrosis.

Lymph nodes mapping

Mice were anesthetized with 2.5% isoflurane and injected subcutaneously with 5% Evans blue (Sigma) dye into the front legs, the hindfoot and the ears. After 30 minutes of continuous anesthesia, mice were euthanized and dissected to locate the lymph nodes[27].

Statistical analysis

Statistical significance was calculated with a two-tailed Mann & Whitney test using Prism software (GraphPad) except for the survival curves which were evaluated using Kaplan-Meier analysis (Log-rank test). All data were presented as mean ± Standard Error of the Mean (SEM). P-values < 0.05 were considered statistically significant (*, $p<0.05$, **, $p<0.01$, ***, $p<0.001$, ****,$p<0.0001$).

RESULTS

Heterozygous Sting V154M mice demonstrate marked weight loss and reduced survival

Heterozygous mutations in STING, including V155M mutation (V154M in mice), are responsible for the development of SAVI[15,16]. We generated heterozygous V154M mice using CRISPR/Cas9 technology, by inserting an oligonucleotide containing two mutations (GTT into ATG, resulting in the replacement of a valine 154 with a methionine) into exon 5 of *Tmem173* (Fig 1, A, green and red). In order to facilitate genotyping, the oligonucleotide also contained a silent mutation encoding for a NcoI restriction site (Fig 1, A, yellow). In this way, Sting V154M/WT mice could be distinguished from wild-type (WT) animals by PCR (Fig 1, B). We confirmed the presence of the mutation by Sanger sequencing of genomic DNA and complementary DNA (Fig 1, C). We also analyzed Sting expression in this model. It has been shown that STING expression is decreased in HEK293FT cells transfected with the V155M STING mutation in comparison with cells expressing WT STING[7,16]. In agreement with this, we noticed a reduction of nearly 50% of *Sting* mRNA and Sting protein in Sting V154M/WT mice (Fig S1, A and B).

Interestingly, V154M/WT mice showed a marked reduction in survival compared to WT littermates, with none surviving beyond 150 days (Fig 1, D). Such a high mortality rate precluded analysis in our animal facility conditions. Therefore, because the mice were not raised in a germ-free environment, we treated them with enrofloxacin, a broad-spectrum antibiotic. Survival was then significantly improved (Fig, 1D), but Sting V154M/WT mice still exhibited weight loss compared to WT littermates (Fig S1, C). Sting V154M/WT females were sterile, hence we were unable to breed mice homozygous for the Sting V154M allele.

Sting V154M/WT mice variably develop lung and renal inflammation.

SAVI is characterized by an inflammatory state[15,16]. In particular, lung interstitial disease has been observed in the majority of patients, as well as skin lesions, and systemic inflammation. These features are not present in all patients, with rare familial cases of the disease confirming sometimes marked variability in disease expression[16]. We noticed that 45% of Sting V154M/WT mice developed slight (++) to severe (++++) alveolar or perivascular inflammation, whereas none of the WT littermate group developed these features (Fig S2). Of note, we did not detect any lung fibrosis (Fig S2), nor did our mice demonstrate skin lesions, arthritis or inflammation in the distal limbs (Fig S2). Almost thirty percent of the mice developed a minimal renal inflammation (interstitial hypercellularity in the medulla), with some patches of

interstitial fibrosis, whereas WT littermate mice didn't develop any. However, similar lesions have not been reported in human SAVI patients. Proteinuria was not recorded in the Sting V154M/WT mice. We did not observe any correlation between organ inflammation in Sting V154M/WT mice according to whether they were treated or not with antibiotic (Fig S2). In addition, there was a significant increase in serum interleukin 6 (IL-6) and tumor necrosis factor α (TNF-α) levels in mutant animals compared to WT littermates (1.2 ± 0.003 pg/mL *versus* 20.8 ± 8.1 pg/mL for IL6, 3.8 ± 0.003 pg/mL *versus* 5.7 ± 1.2 pg/mL for TNFα, in WT and Sting V154M/WT mice, respectively, mean ± SEM; $p<0.05$, Mann and Whitney test). Thus we conclude that Sting V154M/WT mice developed inflammatory manifestations with variable expression.

Sting V154M/WT mice develop severe combined immunodeficiency (SCID).

Considering the T cell lymphopenia observed in SAVI patients[15,16], we analyzed the proportion of immune cell subsets in peripheral lymphoid compartments. Because survival was improved after treatment with enrofloxacin, all of the animals included in this analysis had received antibiotic. Firstly, we noticed a complete absence of lymph nodes (LNs) in Sting V154M/WT mice, even after coloration with Evans blue (Fig S3). In addition, we saw a significant decrease in white blood cell counts in Sting V154M/WT mice compared to WT littermates (Fig 2, A). Flow cytometry analysis showed that the distribution of blood leucocyte subpopulations was different in Sting V154M/WT compared to WT animals, with a decrease of B, CD4+ and CD8+ T cells, and NK cells, associated with an increase of granulocytes and monocytes (Fig 2, A). Furthermore, Sting V154M/WT mice developed anemia (Fig 2, B), consistent with the description in SAVI patients[15,16], possibly reflecting systemic inflammation. In accordance with the blood analysis, the spleens of Sting V154M/WT mice demonstrated a severe reduction in B cells, CD4+ and CD8+ T cells, and NK cells, both in terms of percentage and absolutes numbers, particularly affecting T and NK cells. All B cell subsets (follicular, transitional T1 and T2, and marginal zone B cells) were also affected (Fig 2, C). The same observation was made for T cell subsets, where we recorded a decrease in effector memory, central (markedly in CD8+ T cells) and naïve T cells, the latter being the most impacted T cell subpopulation (Fig 2, C). The regulatory T cell compartment (Tregs) was also impacted (Fig. S4). However, even if the percentage and absolute number of Tregs was strongly diminished (Fig. S4, A), the ratio of Tregs on total CD4+ T cells remained unchanged between Sting V154M/WT and WT littermate mice. Furthermore, the expression of functional marker CD25 on Tregs was comparable

between WT and Sting V154M/WT mice (Fig S4, B). In addition to the dramatic decrease in all lymphoid populations, we noticed a significant increase of granulocyte and monocyte populations in the Sting V154M/WT mice (percentages and absolute numbers) (Fig 2, C). In agreement with these latter results, we detected an excess of serum MCP-1 (monocyte chemotactic protein-1 or CCL2) production in the serum of Sting V154M/WT mice (3.9 ± 0.7 pg/mL *versus* 47.6 ± 13.2 pg/mL in WT and Sting V154M/WT mice, respectively, mean ± SEM ; $p<0.05$, Mann and Whitney test). Finally, consistent with the reduction in B cells, total immunoglobulin (Ig) M and IgG levels were profoundly decreased in serum Sting V154M/WT mice in comparison to WT littermates, and IgA was undetectable (Fig 2, D). The introduction of the V154M heterozygous mutation in mice was thus responsible for the development of a SCID phenotype, affecting all lymphocyte populations, associated with a severe hypogammaglobulinemia, and a developmental defect of LNs.

The B- and T-cell developmental blockade in Sting V154M/WT mice originates at the early immature stages in bone marrow and thymus.

In order to understand the mechanisms of lymphocyte deficiency in the periphery, we analyzed early developmental stages in the bone marrow (BM) and thymus. The Hematopoietic stem cell (HSC) compartment in the BM, containing long-term HSC (LT-HSC), short-term HSC (ST-HSC), and multipotent progenitors (MPP), was not affected by the Sting V154M mutation (Fig S5, A). Similarly, the percentages and absolute numbers of common lymphoid progenitors (CLP) were comparable in the two groups of mice (Fig S5, B). However, T and B cell lineages were markedly affected after the CLP stage. Indeed, Sting V154M/WT mice displayed a strong reduction in ProB and PreB subsets, and an even more profound decrease in immature and mature stages (Fig 3, A). These results indicated that a developmental arrest between CLP and further stages of B cell subsets is responsible for the peripheral B cell lymphopenia. In addition, thymic T cell development seemed to be very impacted since Sting V154M/WT mice presented a residual thymus consistent with markedly reduced cellularity (Fig 3, B). Percentages and absolute numbers of early thymic progenitors (ETP) were comparable between Sting V154M/WT and control animals (Fig 3, C). However, thymocyte development was profoundly impaired at the double negative (DN) 1 and DN2 stages, and to a lesser extent at subsequent stages (Fig 3, C). Finally, the absolute numbers of double positive (DP) and CD4 and CD8 single positive thymocytes were decreased in Sting V154M/WT mice (Fig 3, D), thus explaining the peripheral T-cell lymphopenia. In order to analyze in more detail the mechanisms of this lymphopenia, we also assessed the proliferation and death status in

progenitors both from BM and thymus, using annexin V and BrdU staining (Fig 3, E and F). We observed that progenitors from B and T cell lineages are more prone to die by apoptosis (Fig 3, E). We also observed an increased incorporation of BrdU indicating an increased proliferation (Fig 3, F). We thus think that the increased apoptosis of lymphoid progenitors is possibly accounting for the observed peripheral lymphopenia in Sting V154M/WT mice. Considering the myeloid population and consistent with their expansion in periphery, we also observed an increased percentage of monocytes in the BM (Fig S5, C). However, we did not detect any increase in common myeloid progenitors (CMP) and granulocyte-monocyte progenitors (GMP) (Fig S5, B), suggesting a homeostatic peripheral expansion of the myeloid compartment as a consequence of impaired lymphocyte development. Finally, a slight reduction of erythrocytes was noticed in the BM of mutant mice (Fig S5, D). Percentages and absolute numbers of megakaryocyte and erythroid progenitors (MEP) and pro-erythroblasts were not statistically different between the 2 groups of mice (Fig S5, B and D). This anemia could therefore be a consequence of inflammation, or of a slight blockade in erythrocyte development between the pro-erythroblast and erythrocyte stages, or both. In conclusion, the profound T and B cell lymphopenia observed in Sting V154M/WT mice is at least partly a consequence of an early developmental defect characterized by an increased apoptosis of progenitors.

Sting V154M mutation results in intrinsic defects in mature T and B cells.

Because of the T and B cell lymphopenia and reduced antibody levels in Sting V154M/WT mice (Fig. 2), we further investigated the expression of activation markers and the proliferative response of these cells after *in vitro* stimulation. We detected a 6-fold increase of the CD86 activation marker on unstimulated Sting V154M/WT B cells compared to WT counterparts. Overexpression of the CD86 marker was also observed after stimulation with anti-CD40 and IL-4, or with anti-IgM and anti-CD40 (Fig 4, A). Considering the profound hypogammaglobulinemia in Sting V154M/WT mice (Fig 2, D), we quantified the secreted Ig in supernatant after stimulation of total splenocytes *in vitro*. Immunoglobulin secretion was strongly decreased in supernatants from Sting V154M/WT splenocytes, after stimulation with LPS, LPS and IL-4 or anti-CD40 and IL-4 (Fig 4, B). This was not the consequence of an intrinsic defect of proliferation or plasma cell differentiation (Fig 4, C and D). However, Sting V154M/WT B cells were significantly more sensitive to apoptosis than WT B cells, as shown by annexin V staining after 2 days of stimulation, with several protocols of stimulation, including those mimicking T cell help (Fig 4, E). Similar to B cells, splenic $CD4^+$ and $CD8^+$ T

cells displayed a hyperactivated profile at steady-state, illustrated by an overexpression of the CD25 activation marker (Fig 5, A). Sting V154M/WT T cells also displayed a profound activation defect following stimulation with anti-CD3 and anti-CD28 (Fig 5, A) along with decreased proliferation and increased cell necrosis and apoptosis (Fig 5, B and C). These results showed that mature T cells from Sting V154M/WT mice have an intrinsic proliferative defect that cannot compensate the increased mortality. Thus, the very low production of immunoglobulins *in vivo* could be the combined consequence of an increased B and T cell apoptosis leading to a low number of B and T cells, and a lack of T cell help required for B cell activation and differentiation into plasma cells.

The SCID observed in Sting V154M/WT mice is type I IFN-independent.

Given that aspects of the SAVI phenotype have been proposed to reflect enhanced type I IFN signaling, we analyzed the expression of ISGs in Sting V154M/WT mice. The expression of *Isg15*, *Ifit1*, and *Cxcl10/IP10* was significantly increased in total splenocytes (Fig 6, A) and confirmed in splenic sorted B cells from Sting mutant mice (Fig 6, B). The expression of IFNα and IFNβ was also higher in these cells (Fig 6, B), as expected with a Sting GOF mutation. In order to evaluate the impact of excessive type-I IFN production on the phenotype of Sting V154M/WT mice, we bred them with IFNAR knock-out (KO) animals. Expectedly, the expression of ISGs returned to basal levels in Sting V154M/WT IFNAR KO animals (Fig 6, A). However, the weight loss (Fig 6, C), the hypogammaglobulinemia (Fig 6, D), the SCID phenotype (decrease of B, T and NK cells) and the expansion of monocytes and granulocytes, were not reversed (Fig 6, E). This indicated that the blockade in T, B and NK cell development observed in Sting V154M/WT mice is not type I IFN-dependent. However, the anti-proliferative and pro-death effect of the Sting V154M mutation in T cells was partially reversed in double-mutant animals (Fig 6, F and G), thus indicating both IFN dependent and independent effects of Sting GOF.

CONCLUSIONS

The development of a lymphopenia affecting T and NK cells is a common feature of patients carrying a STING V155M mutation, and other mutations such as N154S or V147L[15,16]. Total B cell counts in these patients are in the normal range, although memory and switched memory B cells are decreased[15,16]. IgG and IgA hypergammaglobulinemia is seen in several patients with SAVI. Our data demonstrate that the introduction of a Sting V154M mutation in mice (corresponding to the V155M mutation in humans) leads to the development of a SCID phenotype (T, B and NK lymphopenia), more profound than that so far described in any SAVI patient, as well as an important growth delay and a dramatic reduction in survival. These mice also demonstrated a marked IgM, IgG and IgA hypogammaglobulinemia. We conclude that both the T and B cell lymphopenia are at least partly the consequence of a blockade in early T and B cell progenitor development, therefore highlighting an unforeseen role of STING in the lymphoid development. Proliferation and apoptosis analyses performed on V154M/WT lymphocyte progenitors showed both proliferative expansion and increased apoptosis. Therefore, the increased apoptosis of lymphoid progenitors is possibly accounting for the observed peripheral lymphopenia in Sting V154M/WT mice. Similar observations have been previously made in different systems like *Drosophilia* or Mouse Embryonic Fibroblasts[28-30] where authors concluded on a causal link between apoptosis and proliferation. Indeed, a compensatory proliferation after cell death can be triggered by caspases and be responsible for the induction of adjacent surviving cells proliferation in order to replace dying cells[28,29,31]. Moreover, Cabatingan *et al*. have proposed a mechanism in which homeostatic B cell proliferation is a regulatory process related to the intrinsic B cell defect[32]. Further experiments, such as transcriptome analysis in successive stages of B and T development, are needed to better understand the developmental arrest of lymphoid progenitors in Sting V154M/WT mice.

Several hypotheses can be proposed to explain the lymphocyte development blockade observed in Sting V154M/WT mice but not in SAVI patients. Firstly, the level of STING expression could be different in early T and B cell progenitors between humans and mice. Secondly, one can speculate that partners of STING and/or target genes implicated in lymphocyte development are distinct between species. These potential differences may lead to a toxic effect on lymphoid progenitors that is more pronounced in mice, or not reversed by compensatory mechanisms existing in humans.

In addition, we observed an absence of LNs in Sting V154M/WT mice. This could be, at least in part, the consequence of an absence of Lymphoid Tissue-inducing cells (LTi), members of an emerging family of innate lymphoid cells (ILCs) which play a key role in the development

of LNs and Peyer's patches. ILCs develop from the CILP (common innate lymphoid progenitor) stage coming from CLP progenitor in bone marrow[33]. Therefore, considering the blockade of lymphoid cells development in Sting V154M/WT mice after the CLP stage, one could speculate that the ontogeny of ILCs is also impacted. In addition, lymphotoxin alpha (LTα) deficient mice are also lacking LN, demonstrating an important role for LTi-derived LTα in secondary lymphoid organ development during embryogenesis[34-36]. Preliminary results confirmed that the expression of LTα is decreased in T cells from Sting V154M/WT mice.

Finally, mature B and T cells displayed intrinsic defects, characterized by a hyperactivation status at steady state, and by a defect of activation and proliferation in mature T cells. We showed that the hypogammaglobulinemia was not the consequence of a B-cell intrinsic proliferation or differentiation defect. However, we detected an increase of apoptosis in B and T cells. It is therefore plausible that the low Ig titers accompanying B cell lymphopenia relate to a lack of T cell help.

Another common molecular feature of the SAVI phenotype, for all the mutations described so far, is an increased expression of ISGs. In Sting V154M/WT mice, we detected a significant IFN signature in splenocytes and in sorted B cells. The magnitude of the IFN signature in our mice (almost 5 fold) is close to that described in murine models of the type I interferonopathy Aicardi-Goutières syndrome, carrying the homozygous RNaseH2 G37S point mutation[37, 38], and animals deficient for *Samhd1*[39]. To our surprise, the KO of IFNAR in Sting V154M/WT mice rescued neither the defect in B, T, and NK cell development, nor the profound hypogammaglobulinemia, and did not reverse the expansion of myeloid cells, suggesting that type I IFN does not play a causal role in the SCID phenotype of Sting V154M/WT mice. However, the *in vitro* proliferative defect and the pro-death phenotype of mature T cells were partially reversed by IFNAR deficiency. These data suggest potential multiple effects of Sting GOF, comprising a type I IFN-independent blockade of lymphocyte development at early stages on one hand, and an anti-proliferative effect in T cells which is partially type I IFN-dependent on the other hand. A defect of T cell proliferation in SAVI patients has been described recently, but was not reversed by type I IFN or TNF neutralization *in vitro*[40]. One difference between the two experimental models is the fact that T cells in our mutant mice developed in an *in vivo* IFNAR KO environment, as opposed to an *ex vivo* / *in vitro* setting. In addition, one cannot exclude the existence of species-specific mechanisms in the control of T cell proliferation through the STING/type I IFN pathway. Finally, our data showed that the

partial rescue of the anti-proliferative effect of Sting in IFNAR KO T cells could not reverse the low Ig production recorded in Sting V154M/WT mice.

We observed some inflammatory manifestations in Sting V154M/WT mice, although with variable expression. These included signs of pulmonary and renal inflammation in 45% and 27% of the animals, respectively, which was associated to an increased production of inflammatory cytokines. We did not record any lung fibrosis, or skin lesions, which is distinct from the overall clinical picture of SAVI. The variable penetrance of pulmonary and renal inflammation is in accordance with the human disease state which is also characterized by variable expression, spanning early-onset systemic inflammation with mutilating skin lesions and lethal pulmonary inflammation[15,16], through to "idiopathic" lung fibrosis[21,23] and isolated chilblain lupus inherited stably across several generations[24]. In addition, an intrafamilial disease expression variability is also observed in humans[16]. The inconstant expression of organ inflammation in Sting V154M/WT model suggests that environmental factors (animal facility environment and potential interaction with microbiota) are needed. Moreover, these results confirmed that renal damages observed are not a consequence of the long-term antibiotic treatment, as only some mutant mice (27%), but none of the treated controls, presented with kidney inflammation.

Warner *et al*. recently described another model of Sting GOF, the N153S model, corresponding to the N154S mutation in SAVI patients[41]. These mice developed an inflammatory disease with pulmonary inflammation ~~(lung involvement in 20% of animals)~~ in the absence of fibrosis, and skin inflammation, associated with an immune deficiency, including T cell lymphopenia. They concluded that some features of N153S mice were different from those seen in STING N154S SAVI patients. Altogether, the data obtained from Sting GOF mutations in mice (N153S and V154M) are in support of partial differential effects of STING pathway in humans and mice. The two animal models have common characteristics, such as T and NK cell lymphopenia, and the existence of inflammatory features. The anti-proliferative effect of Sting N153S GOF was not assessed by Warner *et al*. but an *in vitro* proliferative defect is seen both in the STING V155M[16] and in STING N154S human lymphocytes (F. Rieux-Laucat, unpublished results). However, some differences between the Sting N153S and V154M models are also observed. Indeed, the Sting V154M mice described here are characterized by a B cell lymphopenia and a marked hypogammaglobulinemia, whereas Sting N153S mice demonstrated normal B cell counts and hyper IgM. This hyperproduction, in the context of a T cell lymphopenia in Sting N153S mice, is not explained for the moment, but it may possibly relate to a defective T-B cooperation in germinal centers. The lack of hyper IgM in the V154M model suggests that B

cell precursors are more affected than those of the N153S model. Whether it relates to differential expression levels of the mutants or to different impacts on STING partners remains to be established. Finally, the expression of organic lesions was also different between the two models. It has been shown that human N154S and V155M mutations result in constitutive ER STING exit, and thus activate STING independently of cGAMP binding[14]. Moreover, both mutations are localized in the DD domain of STING and form constitutive and stable dimers [15,16]. However, some mutation-dependent effects might be envisaged to explain the phenotypic differences between these two models. Further experiments (such as genome-wide transcriptome profiling) comparing N153S and V154M murine cells will be necessary to elucidate such differences. One may also questioned a possible difference in the stability of the two mutant proteins. In addition, considering the important role of STING in viral and bacterial sensing, we cannot exclude differences in environmental factors (animal facility environment and health status) between the two models. The survival of the V154M/WT mice was statistically increased after treatment with enrofloxacin, a broad-spectrum antibiotic, perhaps arguing in favor of a microbial-dependent effect. However, an extensive bacteriological analysis did not detect any infection related to pathogens targeted by this antibiotic in our mice. An alternative possibility is that enrofloxacin treatment had an effect on the intestinal microbiota composition, and that Sting interaction with the microbiotia can impact on the mice phenotype, notably because STING is activated by cyclic dinucleotides and that such CDNs can be produced by gut microbiota[42, 43]. Indeed, STING seems to be highly implicated in the gut homeostasis, as shown in Sting deficient mice[42]. Thus, we can suppose that a fine regulation of Sting is necessary to maintain this homeostasis and would explain variations between mice, depending on interactions with the environment. Moreover, authors showed that IgA seem to be essential for gut homeostasis, since they decrease the commensal bacteria penetration in the intestinal epithelium[42]. Therefore, IgA deficiency in our GOF model could also have an impact on intestinal microbiota and gut homeostasis.

Considering these findings, this new mouse model constitutes an important model in which to explore the role of Sting in lymphocyte development, and to further improve our understanding of pathophysiological mechanisms of lymphopenia in SAVI patients on the one hand, and of SCID (including severe hypogammaglobulinemia) on the other. Finally, the type-I IFN independent mechanism of SCID development may have important implications in the future treatment strategy of SAVI patients.

ACKNOWLEDGMENTS

We thank D. Bock, M. Duval, D. Lamon, S. Reibel-Foisset and K. Sablon for excellent animal care. We thank V. Flacher, F. Gros and C. Mueller (CNRS UPR 3572 "Immunopathology and Therapeutic Chemistry"/Laboratory of Excellence Medalis, Institute of Molecular and Cellular Biology (IBMC), Strasbourg, France) for scientific discussions. YJC acknowledges the European Research Council (GA 309449: Fellowship to YJC).

This work was supported by grants from Strasbourg University (UdS), Centre National de la Recherche Scientifique (CNRS), by the Agence Nationale de la Recherche (ANR-14-CE14-0026-04, Lumugene; and ANR-11-EQPX-022) and by EU-funded (ERDF) project INTERREG V "RARENET". D.B. and F.A. were supported by the Ministère de la Recherche et de la Technologie. V.D. was supported by Initiative of Excellence (IdEx), Strasbourg University, France.

AUTHOR CONTRIBUTIONS

D.B., T.M., A.S.K., F.R.L. and P.S.S. designed the research.
D.B., F.A., D.L., V.D., C.E., H.J., and A.M.K. performed the research.
D.B., P.K., S.J., H.J., N.J., Y.J.C., I.A.S., A.S.K., F.R.L. and P.S.S. analyzed the data.
D.B., S.J., A.B., Y.J.C., I.A.S., A.S.K., F.R.L. and P.S.S. wrote the paper.

635 **REFERENCES**

636 1. Ishikawa H, Barber GN. STING is an endoplasmic reticulum adaptor that facilitates innate
637 immune signalling. Nature. 2008 Oct 2;455(7213):674–8.

638 2. Jin L, Waterman PM, Jonscher KR, Short CM, Reisdorph NA, Cambier JC. MPYS, a novel
639 membrane tetraspanner, is associated with major histocompatibility complex class II and
640 mediates transduction of apoptotic signals. Mol Cell Biol. 2008 Aug;28(16):5014–26.

641 3. Sun W, Li Y, Chen L, Chen H, You F, Zhou X, et al. ERIS, an endoplasmic reticulum IFN
642 stimulator, activates innate immune signaling through dimerization. Proc Natl Acad Sci USA.
643 2009 May 26;106(21):8653–8.

644 4. Zhong B, Yang Y, Li S, Wang Y-Y, Li Y, Diao F, et al. The adaptor protein MITA links
645 virus-sensing receptors to IRF3 transcription factor activation. Immunity. 2008 Oct
646 17;29(4):538–50.

647 5. Marinho FV, Benmerzoug S, Oliveira SC, Ryffel B, Quesniaux VFJ. The Emerging Roles
648 of STING in Bacterial Infections. Trends Microbiol. 2017 Nov;25(11):906–18.

649 6. Cai X, Chiu Y-H, Chen ZJ. The cGAS-cGAMP-STING pathway of cytosolic DNA sensing
650 and signaling. Mol Cell. 2014 Apr 24;54(2):289–96.

651 7. Melki I, Rose Y, Uggenti C, Van Eyck L, Frémond M-L, Kitabayashi N, et al. Disease-
652 associated mutations identify a novel region in human STING necessary for the control of type
653 I interferon signaling. J Allergy Clin Immunol. 2017 Aug;140(2):543–552.e5.

654 8. Barber GN. STING-dependent cytosolic DNA sensing pathways. Trends Immunol. 2014
655 Feb;35(2):88–93.

656 9. Panday A, Inda ME, Bagam P, Sahoo MK, Osorio D, Batra S. Transcription Factor NF-κB:
657 An Update on Intervention Strategies. Arch Immunol Ther Exp (Warsz). 2016 Dec;64(6):463–
658 83.

659 10. Chen H, Sun H, You F, Sun W, Zhou X, Chen L, et al. Activation of STAT6 by STING is
660 critical for antiviral innate immunity. Cell. 2011 Oct 14;147(2):436–46.

661 11. Burdette DL, Vance RE. STING and the innate immune response to nucleic acids in the
662 cytosol. Nat Immunol. 2013 Jan;14(1):19–26.

663 12. Ahn J, Gutman D, Saijo S, Barber GN. STING manifests self DNA-dependent
664 inflammatory disease. Proc Natl Acad Sci USA. 2012 Nov 20;109(47):19386–91.

665 13. Roers A, Hiller B, Hornung V. Recognition of Endogenous Nucleic Acids by the Innate
666 Immune System. Immunity. 2016 Apr 19;44(4):739–54.

667 14. Dobbs N, Burnaevskiy N, Chen D, Gonugunta VK, Alto NM, Yan N. STING Activation
668 by Translocation from the ER Is Associated with Infection and Autoinflammatory Disease. Cell
669 Host Microbe. 2015 Aug 12;18(2):157–68.

670 15. Liu Y, Jesus AA, Marrero B, Yang D, Ramsey SE, Sanchez GAM, et al. Activated STING
671 in a vascular and pulmonary syndrome. N Engl J Med. 2014 Aug 7;371(6):507–18.

16. Jeremiah N, Neven B, Gentili M, Callebaut I, Maschalidi S, Stolzenberg M-C, et al. Inherited STING-activating mutation underlies a familial inflammatory syndrome with lupus-like manifestations. J Clin Invest. 2014 Dec;124(12):5516–20.

17. Crow YJ. Type I interferonopathies: a novel set of inborn errors of immunity. Ann N Y Acad Sci. 2011 Nov;1238:91–8.

18. Rodero MP, Crow YJ. Type I interferon-mediated monogenic autoinflammation: The type I interferonopathies, a conceptual overview. J Exp Med. 2016 Nov 14;213(12):2527–38.

19. Munoz J, Rodière M, Jeremiah N, Rieux-Laucat F, Oojageer A, Rice GI, et al. Stimulator of Interferon Genes-Associated Vasculopathy With Onset in Infancy: A Mimic of Childhood Granulomatosis With Polyangiitis. JAMA Dermatol. 2015 Aug;151(8):872–7.

20. Omoyinmi E, Melo Gomes S, Nanthapisal S, Woo P, Standing A, Eleftheriou D, et al. Stimulator of interferon genes-associated vasculitis of infancy. Arthritis & Rheumatology (Hoboken, NJ). 2015 Mar;67(3):808.

21. Clarke SLN, Pellowe EJ, de Jesus AA, Goldbach-Mansky R, Hilliard TN, Ramanan AV. Interstitial Lung Disease Caused by STING-associated Vasculopathy with Onset in Infancy. Am J Respir Crit Care Med. 2016 01;194(5):639–42.

22. Frémond M-L, Rodero MP, Jeremiah N, Belot A, Jeziorski E, Duffy D, et al. Efficacy of the Janus kinase 1/2 inhibitor ruxolitinib in the treatment of vasculopathy associated with TMEM173-activating mutations in 3 children. J Allergy Clin Immunol. 2016 Dec;138(6):1752–5.

23. Picard C, Thouvenin G, Kannengiesser C, Dubus J-C, Jeremiah N, Rieux-Laucat F, et al. Severe Pulmonary Fibrosis as the First Manifestation of Interferonopathy (TMEM173 Mutation). Chest. 2016 Sep;150(3):e65-71.

24. König N, Fiehn C, Wolf C, Schuster M, Cura Costa E, Tüngler V, et al. Familial chilblain lupus due to a gain-of-function mutation in STING. Ann Rheum Dis. 2017 Feb;76(2):468–72.

25. Müller U, Steinhoff U, Reis LF, Hemmi S, Pavlovic J, Zinkernagel RM, et al. Functional role of type I and type II interferons in antiviral defense. Science. 1994 Jun 24;264(5167):1918–21.

26. Schickel JN, Pasquali JL, Soley A, Knapp AM, Decossas M, Kern A, et al. Carabin deficiency in B cells increases BCR-TLR9 costimulation-induced autoimmunity. EMBO Mol Med. 2012;4(12):1261-75.

27. Harrell MI, Iritani BM, Ruddell A. Lymph node mapping in the mouse. J Immunol Methods. 2008 Mar 20;332(1–2):170–4.

28. Fan Y, Bergmann A. Apoptosis-induced compensatory proliferation. The Cell is dead. Long live the Cell! Trends Cell Biol. 2008 Oct;18(10):467–73.

29. Fan Y, Wang S, Hernandez J, Yenigun VB, Hertlein G, Fogarty CE, et al. Genetic models of apoptosis-induced proliferation decipher activation of JNK and identify a requirement of EGFR signaling for tissue regenerative responses in Drosophila. PLoS Genet. 2014 Jan;10(1):e1004131.

711 30. Fogarty CE, Bergmann A. Killers creating new life: caspases drive apoptosis-induced
712 proliferation in tissue repair and disease. Cell Death Differ. 2017;24(8):1390–400.

713 31. Ryoo HD, Bergmann A. The role of apoptosis-induced proliferation for regeneration and
714 cancer. Cold Spring Harb Perspect Biol. 2012 Aug 1;4(8):a008797.

715 32. Cabatingan MS, Schmidt MR, Sen R, Woodland RT. Naive B lymphocytes undergo
716 homeostatic proliferation in response to B cell deficit. J Immunol. 2002 Dec 15;169(12):6795–
717 805.

718 33. Zook EC, Kee BL. Development of innate lymphoid cells. Nat Immunol. 2016
719 21;17(7):775–82.
720
721 34. Kim M-Y, Kim K-S, McConnell F, Lane P. Lymphoid tissue inducer cells: architects of
722 CD4 immune responses in mice and men. Clin Exp Immunol. 2009 Jul;157(1):20–6.

723 35. Kruglov AA, Grivennikov SI, Kuprash DV, Winsauer C, Prepens S, Seleznik GM, et al.
724 Nonredundant function of soluble LTα3 produced by innate lymphoid cells in intestinal
725 homeostasis. Science. 2013 Dec 6;342(6163):1243–6.

726 36. Lane PJL, Gaspal FM, McConnell FM, Kim MY, Anderson G, Withers DR. Lymphoid
727 tissue inducer cells: innate cells critical for CD4+ T cell memory responses? Ann N Y Acad
728 Sci. 2012 Jan;1247:1–15.

729 37. Pokatayev V, Hasin N, Chon H, Cerritelli SM, Sakhuja K, Ward JM, et al. RNase H2
730 catalytic core Aicardi-Goutières syndrome-related mutant invokes cGAS-STING innate
731 immune-sensing pathway in mice. J Exp Med. 2016 Mar 7;213(3):329–36.

732 38. Mackenzie KJ, Carroll P, Lettice L, Tarnauskaitė Ž, Reddy K, Dix F, et al. Ribonuclease
733 H2 mutations induce a cGAS/STING-dependent innate immune response. EMBO J. 2016 Apr
734 15;35(8):831–44.

735 39. Maelfait J, Bridgeman A, Benlahrech A, Cursi C, Rehwinkel J. Restriction by SAMHD1
736 Limits cGAS/STING-Dependent Innate and Adaptive Immune Responses to HIV-1. Cell Rep.
737 2016 09;16(6):1492–501.

738 40. Cerboni S, Jeremiah N, Gentili M, Gehrmann U, Conrad C, Stolzenberg M-C, et al. Intrinsic
739 antiproliferative activity of the innate sensor STING in T lymphocytes. J Exp Med. 2017 Jun
740 5;214(6):1769–85.

741 41. Warner JD, Irizarry-Caro RA, Bennion BG, Ai TL, Smith AM, Miner CA, et al. STING-
742 associated vasculopathy develops independently of IRF3 in mice. J Exp Med. 2017 Nov
743 6;214(11):3279–92.

744 42. Canesso MCC, Lemos L, Neves TC, Marim FM, Castro TBR, Veloso ÉS, et al. The
745 cytosolic sensor STING is required for intestinal homeostasis and control of inflammation.
746 Mucosal Immunol. 2017 Dec; 20:1-15

747 43. Barber GN. STING: infection, inflammation and cancer. Nat Rev Immunol. 2015
748 Dec;15(12):760–70.

749

FIGURE LEGENDS

Figure 1. Murine *Sting* V154M heterozygous mutation is associated with a reduced survival. (A) Introduction of the murine mutation (V154M), corresponding to V155M *Sting* GOF in humans, using CRISPR/Cas9 technology. **(B)** Agarose gel electrophoresis of PCR amplified products using specific primers in exons 4 and 6 of *Tmem173*. Lane 1: DNA size marker, lane 2: negative control of the PCR reaction, lanes 3-5: WT littermate mice, lanes 6-8: Sting V154M/WT mice. **(C)** Visualisation of the heterozygous V154M mutation by Sanger sequencing of genomic DNA (gDNA, upper panel) and complementary DNA (cDNA, lower panel) from WT littermate (left) and transgenic mice (right). **(D)** Survival rates of Sting V154M/WT mice, untreated and treated with antibiotic (see Materials and Methods), as well as control WT littermate mice (n=15 per group) were evaluated by Kaplan-Meier analysis. The result of the Log-rank test is indicated (***, $p<0.0001$).

Figure 2. Murine *Sting* V154M heterozygous mutation is associated with a profound combined immunodeficiency phenotype. (A) Left: total WBC (white blood cells) count ($x10^3$ cells/µL) (n=5 in each group). Right: percentages of immune cell subpopulations in whole blood cells assessed by flow cytometry ($n\geq9$ in each group). **(B)** Left: RBC (red blood cells) count ($x10^6$ cells/µL). Right: hemoglobin levels (g/dL) (n=5 in each group). **(C)** Flow cytometry phenotypic characterization of splenic cells (indicated both as percentages and absolute numbers) ($n\geq13$ in each group). Upper panel: main splenic populations in the spleen of WT littermate mice (open bars) and Sting V154M/WT mice (black bars). Middle panel, left: B cell subpopulations gated on B220+IgM+ cells, with representative dot plots from WT littermate mice and Sting V154M/WT mice. Gates show Transitional 1 (T1: CD21/CD35^{low} CD23^{low}), Transitional 2 (T2: CD21/CD35^{high} CD23^{high}), Follicular (Fo: CD21/CD35^{int} CD23^{high}), and Marginal Zone (Mz: CD21/CD35^{high} CD23l^{ow}) populations. Middle panel, right: representative dot plots of granulocytes (Gr1^{high}Mac1^{+}), monocytes (Gr1^{int}Mac1^{+}) and NK cells (CD49b^{+}NK1.1^{+}). Lower panel: T cell subpopulations gated on CD4^{+} T cells and CD8^{+} T cells respectively, with representative dot plots from WT littermate and Sting V154M/WT mice. Gates show effector memory (Eff. mem.: CD44^{+} CD62L^{-}), central memory (C. m.: CD44^{high} CD62L^{+}) and naive (CD44^{low} CD62L^{+}) T cell populations. **(D)** Total IgM, IgG and IgA (µg/mL) were measured in serum of WT littermate mice (open squares) and Sting V154M/WT mice (black circles). Each dot represents the result for one animal. ND: non detectable. Mice were 2 to 5 months old. Bars represent the mean +/- SEM. *, $p<0.05$, **, $p<0.01$, ***, $p<0.001$, Mann-Whitney test.

Figure 3. The defect observed in B and T cell populations occurs early in their development in the bone marrow (BM) and the thymus. **(A)** Immunophenotyping of B cells in the BM. Left: representative dot plots from WT littermate and Sting V154M/WT mice. Gates show ProB and PreB (IgM-B220^{low}), Immature (Imm.: IgM+B220^{low}) and Mature (IgM+B220^{high}) B cells. Right: mean +/- SEM of percentages and absolute numbers in WT (open bars) and Sting V154M/WT mice (black bars) (n≥6 in each group). **(B)** Left: total number of thymocytes in WT littermate (open bars) and Sting V154M/WT mice (black bars) (n=17 in each group). Right: pictures illustrating the abnormal thymus observed in Sting V154M/WT mice compared to WT littermates (7 weeks old mice). **(C)** Immunophenotyping of ETP and DN cells in the thymus. Left: representative dot plots from WT and Sting V154M/WT mice. Gates show early T cell progenitors (ETP: Lin$^-$CD44$^+$CD25$^-$ckit$^+$), Double Negative fractions DN1 (Lin$^-$CD44$^+$CD25$^-$), DN2 (Lin$^-$CD44$^+$CD25$^+$), DN3 (Lin$^-$CD44$^-$CD25$^+$) and DN4 (Lin$^-$CD44$^-$CD25$^-$). Right: mean +/- SEM of percentages and absolute numbers in WT littermate (open bars) and Sting V154M/WT mice (black bars) (n≥6 in each group). (**D**) Immunophenotyping of DP and SP cells in the thymus. Left: representative dot plots from WT littermate and Sting V154M/WT mice. Gates show Double Positive fraction (DP: Lin$^-$CD8$^+$CD4$^+$), and Simple Positive fractions (CD4: Lin$^-$CD4$^+$CD8$^-$ / CD8: Lin$^-$CD4$^-$CD8$^+$). Percentages and absolute numbers in WT littermate (open bars) and Sting V154M/WT mice (black bars) (n≥6 in each group). (**E**) Cell death analysis by flow cytometry using annexin V staining. The first graph represents the percentages of annexin V$^+$ cells in CLP, ProB and PreB, Immature and Mature stages in bone marrow. The second graph represents each stage of T cell lineage in thymus. WT littermate mice: open bars; Sting V154M/WT mice: black bars (n=5 in each group) (**F**) Proliferation analysis in progenitors by flow cytometry using BrdU staining. The first graph represents the percentages of BrdU+ cells in bone marrow progenitors and the second one represents thymus progenitors. WT littermate mice: open bars; Sting V154M/WT mice: black bars (n=5 in each group). Mice were 2 to 5 months old. Bars represent the mean +/- SEM *, $p<0.05$, **, $p<0.01$, ***, $p<0.001$, Mann-Whitney test.

Figure 4. Sting V154M/WT B cells display intrinsic functional defects. **(A)** Left: ratio of CD86 MFI gated on B220$^+$ cells after 3 days of culture of sorted splenic B cells, in unstimulated cells (NS) or after stimulation with LPS (10µg/mL), anti-IgM (10µg/mL), anti-CD40 / IL4 (1µg/mL – 5ng/mL) and anti-IgM / antiCD40 (10µg/mL – 1µg/mL) (n≥5 in each group). Right: histograms show representative overlays for WT littermate (white) and Sting V154M/WT mice

(grey). **(B)** Total IgM and IgG (ng/mL) were measured in supernatant after 3 days of culture of total splenocytes from Sting V154M/WT (black bars) or WT littermate mice (open bars) (n>5 in each group), with LPS (10µg/mL), LPS / IL4 (10µg/mL – 5ng/mL) or anti-CD40 / IL4 (1µg/mL – 5ng/mL). ND: non detectable. **(C)** Percentage of proliferating B cells after 4 days of stimulation with a combination of anti-IgM (10µg/mL) and anti-CD40 (1µg/mL) or with LPS (10µg/mL). Histogram shows representative overlays (n=5 in each group). **(D)** Left: percentage of plasmablasts ($B220^{low/-}CD138^{+}$) after 3 days of stimulation of B cells with LPS (10µg/mL). Open bars: WT littermate; black bars: Sting V154M/WT (n=6 in each group). Right: representative dot plots. **(E)** Percentage of B cells apoptosis (Annexin V+ cells) after 2 days of stimulation of splenocytes with LPS (10µg/mL), LPS / IL4 (10µg/mL – 5ng/mL), anti-IgM (10µg/mL), anti-CD40 / IL4 (1µg/mL – 5ng/mL) and anti-IgM / antiCD40 (10µg/mL – 1µg/mL) (n>10 in each group). Mice were 2 to 5 months old. Bars represent the mean +/- SEM. *,p<0.05, **, p<0.01, ***, p<0.001, ****, p<0.0001, Mann-Whitney test.

Figure 5. Sting V154M/WT T cells display intrinsic functional defects. (A) Left: ratio of CD25 MFI gated on CD4+ or CD8+ cells after 3 days of culture of splenocytes, in unstimulated cells (NS) or after stimulation with anti-CD3/anti-CD28 (10µg/mL each) for WT littermate (white) and Sting V154M/WT mice (grey) (n=6 in each group). **(B)** Left: percentage of proliferating T cells after 4 days of stimulation of splenocytes from WT littermate (white) and Sting V154M/WT mice (black) with anti-CD3/anti-CD28 (10µg/mL each) (n≥6 in each group). Right: histograms show representative overlays. **(C)** Left panel: Percentage of T cell death (PI^{+} cells) at steady state and after stimulation of splenocytes with anti-CD3/anti-CD28 (10µg/mL each) for 3 days (n≥6 in each group). Right panel: Percentage of T cell death (Annexin V^{+} cells) at steady state and after stimulation of splenocytes with anti-CD3/anti-CD28 (10µg/mL each) for 2 days (n>10 in each group). Mice were 2 to 5 months old. Bars represent the mean +/- SEM. **, p<0.01, ***, p<0.001, ****, p<0.0001, Mann-Whitney test.

Figure 6. The SCID phenotype in Sting V154M/WT mice is type I IFN-independent, but the anti-proliferative effect in T cells is partly IFN-dependent. (A, B) RT-qPCR analysis of ISG in total splenocytes **(A)** and in sorted mature splenic B cells **(B)** of WT littermate (open bars) Sting V154M/WT (black bars), Sting WT/IFNAR KO (light grey) and Sting V154M/WT/IFNAR KO (dark grey). mRNA levels of 3 ISGs (n≥5 in each group) **(A, B)** and of IFNα and IFNβ (n≥3 in each group) **(B)** were measured by qRT-PCR. **(C)** Weight curves of Sting WT/IFNAR KO mice (light grey squares) and Sting V154M/WT/IFNAR KO mice (dark

grey squares). Each dot represents at least 8 mice. **(D)** Flow cytometry phenotypic characterization of splenic cells from WT/IFNAR KO (light grey) and Sting V154M/WT/IFNAR KO (dark grey) mice (n=10 in each group). Left: bar graphs show the mean +/- SEM of percentages (n=10 in each group). Right: representative dot plots of each population: B cells (IgM^+ $B220^+$), CD4+ T cells ($CD4^+CD8^-$), CD8+ T cells ($CD4^-CD8^+$), Granulocytes (Gr.: $Gr1^{high}Mac1^+$), Monocytes (Mo.: $Gr1^{int}Mac1^+$) and NK cells ($CD49b^+NK1.1^+$). **(E)** Total IgM and IgG (µg/mL) were measured in serum of WT/IFNAR KO (open triangles) and Sting V154M/WT/IFNAR KO mice (grey diamonds). Each dot represents one animal. **(F)** Left: percentage of proliferating T cells after 4 days of stimulation of splenocytes from WT/IFNAR KO mice (light grey) and Sting V154M/WT/IFNAR KO mice (dark grey) with anti-CD3/anti-CD28 (10µg/mL each) (n=10 in each group). Right: histogram shows representative overlays. **(G)** Percentage of T cell death (PI^+ cells) at steady state and after stimulation of splenocytes with anti-CD3/anti-CD28 (10µg/mL each) for 3 days (n=10 in each group). Mice were 2 to 5 months old. Bars represent the mean +/- SEM. *, $p<0.05$, **, $p<0.01$, ***, $p<0.001$, ****, $p<0.0001$. Mann-Whitney test.

Supplemental Figure 1. Weight loss and Sting expression in Sting V154M/WT mice. (A) Detection of Sting by immunoblot analysis on sorted splenic B cells (left: representative gel; right: quantification of Sting expression, n=6 mice in each group). **(B)** Expression of *Sting* mRNA assessed by RT-qPCR after RNA extraction of sorted splenic B cells from WT littermate (open bars) and Sting V154M/WT mice (black bars) ($n\geq4$ in each group). **(C)** Left: weight curves of WT littermate mice (open squares) and Sting V154M/WT mice (black circles). Each dot represents at least 17 mice. Right: representative picture of Sting V154M/WT *versus* WT littermate mouse, both females (age at the analysis: 3 months). Bars represent the mean +/- SEM. *,$p<0.05$, **, $p<0.01$, ****, $p<0.0001$, Mann-Whitney test.

Supplemental Figure 2. Histological analysis showing that Sting V154M/WT mice present incomplete penetrance of a lung and renal inflammatory phenotype. (A) Summary of histological analysis performed on 11 Sting V154M/WT mice *versus* 9 WT littermate mice. Each individual experiment is presented with a different colour in the "mouse ID" column. Some mice were treated with the antibiotic (enrofloxacin, see Materials and Methods), as indicated in the second column. **(B)** Representative pictures of Sting V154M/WT mice with organ damages (left, A, C, and E) and with absence of organ damages (right, B, D, and F). (A-B) Hind paws; (C-D) lungs; and (E-F) kidneys (cortex). (A-D and G-H) H&E staining and (E-

F) Masson's trichrome (fibrosis is demonstrated in blue). Ellipses circle subcutaneous vascular network (SVN) that are occasionally obstructed with cellular material. Dotted arrows indicate inflammatory foci in lung and kidney medulla. Arrows point to fibrosis in renal cortex. A: alveolar parenchyma; B: bone; Br: bronchia; BV: blood vessel; E: epidermis; G: glomeruli HF: hair follicle; T: tubules. Scale bars correspond to 100 µm on (A-B); 500 µm on (C-D) and 250 µm on (E-H).

Supplemental Figure 3. Absence of lymph node in Sting V154M/WT mice compared to WT littermates. Pictures from a WT littermate (left column) and a Sting V154M/WT mouse (right column) (7-week-old mice). (A) auricular LNs. (B) axillary LNs. (C) inguinal LNs. (D) popliteal LNs. LNs (arrow) were labelled with 5% Evans blue dye after subcutaneous injection in front legs, hindfoot and ears. Pictures are representative of three distinct experiments. The phenotype was identical at different ages (7-, 12- and 20-week-old mice).

Supplemental Figure 4. Impact of Sting GOF on Tregs and their activation status. (A) Panel on the left shows representative dot plots of the relevant population, both for WT littermate and Sting V154M/WT mice ($n \geq 10$ in each group). Right: histograms showing percentages and absolute numbers of Tregs ($CD4^+Foxp3^+$) and the ratio Tregs/total CD4+ T cells. WT littermate mice are represented with open bars and Sting V154M/WT mice with black bars. **(B)** Expression of CD25 on Tregs. Histogram showing CD25 MFI ($n \geq 4$ in each group) and a representative overlay. Mice were 2 to 5 months old. Bars represent the mean +/- SEM. ***, $p<0.001$, Mann-Whitney test.

Supplemental Figure 5. Despite a defect in hematopoietic cell development after engagement in the B and T cell lineage, early bone marrow progenitors are not impacted in Sting V154M/WT mice. Each panel on the left shows representative dot plots of the relevant population, both for WT littermate and Sting V154M/WT mice ($n \geq 3$ in each group). Each population is shown in chronological order of appearance in the development in the BM. Percentages (middle) and absolute numbers (right) represented for WT littermate (open bars) and Sting V154M/WT (black bars) mice. **(A)** Left: gates show Long-Term (LT-HSC: $Lin^-Sca1^+ckit^+CD48^-CD150^+$) and Short-Term (ST-HSC: $Lin^-Sca1^+ckit^+CD48^-CD150^-$) Hematopoietic-Stem-Cells, and the Multi-Potent-Progenitor (MPP: $Lin^-Sca1^+ckit^+CD48^+CD150^-$) populations. **(B)** Left: gates show the Common Lymphoid (CLP: $Lin^-CD127^{high}ckit^{low}Sca1^{low}$), the Common myeloid (CMP: $Lin^-ckit^+Sca1^-CD16/32^{int}CD34^{int}$),

the Granulocyte/Macrophage (GMP: $Lin^{-}ckit^{+}Sca1^{-}CD16/32^{high}CD34^{high}$) and the Megakaryocyte/erythrocyte (MEP: $Lin^{-}ckit^{+}$ $Sca1^{-}CD16/32^{-}CD34^{-}$) progenitor. **(C)** Left: gates show conventional Dendritic cells (DCs: $CD317^{+}CD11c^{+}$), plasmacytoid Dendritic Cells (pDCs: $CD317^{+}CD11c^{+}$), Monocytes (Mo.: $Gr1^{int}Mac1^{+}$) and Granulocytes ($Gr1^{high}Mac1^{+}$) populations. **(D)** Left: gates represent the megakaryocyte/erythrocyte lineage with Pro-erythrocytes (Pro Er.: $CD71^{+}Ter119^{low}$) and Erythrocytes (Er.: $CD71^{+}Ter119^{+}$).

Bars represent the mean +/- SEM. **, $p<0.01$, Mann-Whitney test.

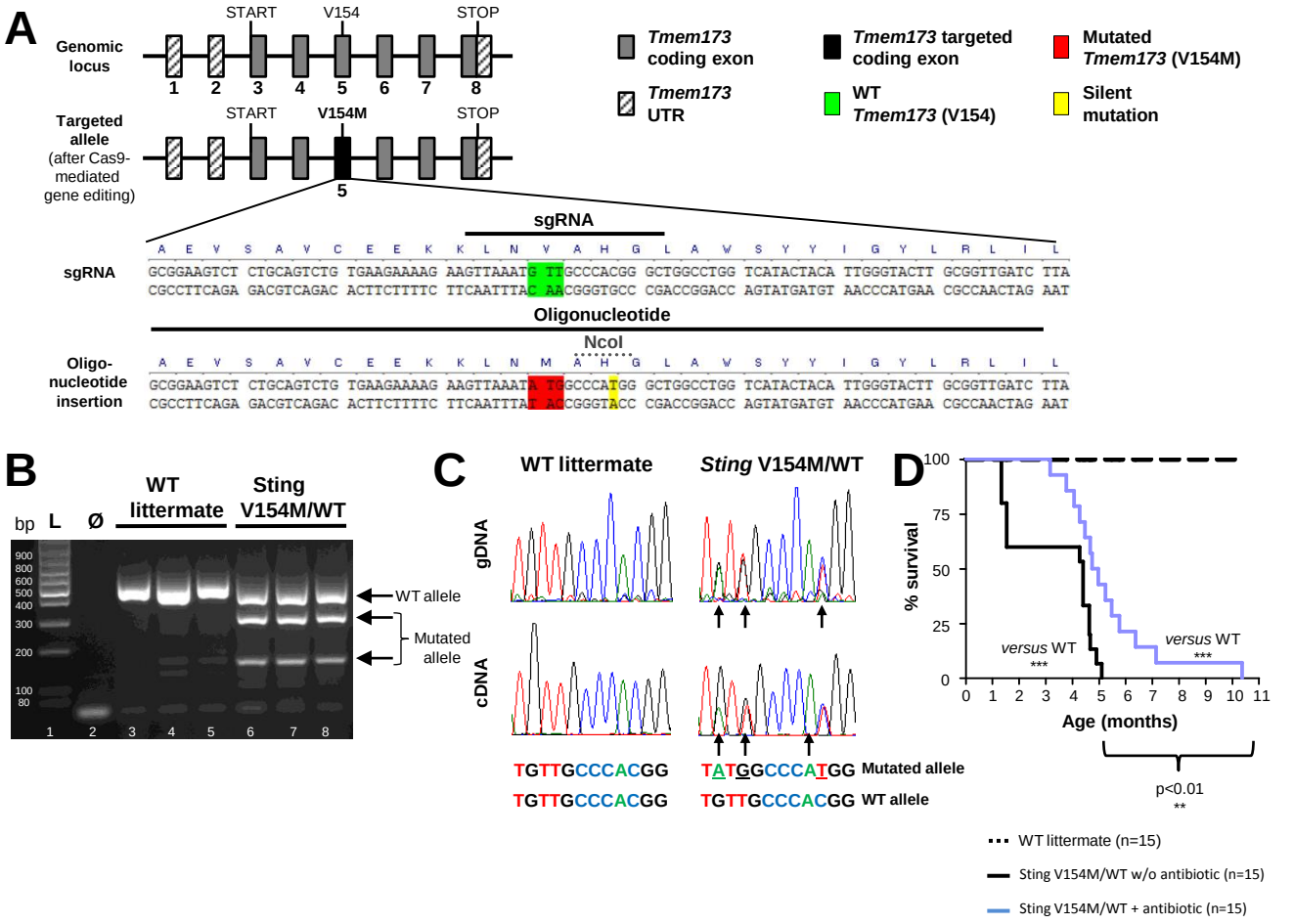
A
Genomic locus
START
V154
STOP
1 2 3 4 5 6 7 8
Targeted allele (after Cas9-mediated gene editing)
START
V154M
STOP
5
Tmem173 coding exon
Tmem173 UTR
Tmem173 targeted coding exon
WT Tmem173 (V154)
Mutated Tmem173 (V154M)
Silent mutation
sgRNA
sgRNA
A E V S A V C E E K K L N V A H G L A W S Y Y I G Y L R L I L
GCGGAAGTCT CTGCAGTCTG TGAAGAAAAG AAGTTAAATG TTGCCCACGG GCTGGCCTGG TCATACTACA TTGGGTACTT GCGGTTGATC TTA
CGCCTTCAGA GACGTCAGAC ACTTCTTTTC TTCAATTTAC AACGGGTGCC CGACCGGACC AGTATGATGT AACCCATGAA CGCCAACTAG AAT
Oligonucleotide
NcoI
Oligo-nucleotide insertion
A E V S A V C E E K K L N M A H G L A W S Y Y I G Y L R L I L
GCGGAAGTCT CTGCAGTCTG TGAAGAAAAG AAGTTAAATA TGGCCCATGG GCTGGCCTGG TCATACTACA TTGGGTACTT GCGGTTGATC TTA
CGCCTTCAGA GACGTCAGAC ACTTCTTTTC TTCAATTTAT ACCGGGTACC CGACCGGACC AGTATGATGT AACCCATGAA CGCCAACTAG AAT
B
WT littermate
Sting V154M/WT
bp
L
Ø
900
800
600
500
400
300
200
100
80
1 2 3 4 5 6 7 8
WT allele
Mutated allele
C
WT littermate
Sting V154M/WT
gDNA
cDNA
TGTTGCCCACGG
TATGGCCCATGG Mutated allele
TGTTGCCCACGG
TGTTGCCCACGG WT allele
D
% survival
100
75
50
25
0
0 1 2 3 4 5 6 7 8 9 10 11
Age (months)
versus WT
***
versus WT
***
p<0.01
**
WT littermate (n=15)
Sting V154M/WT w/o antibiotic (n=15)
Sting V154M/WT + antibiotic (n=15)

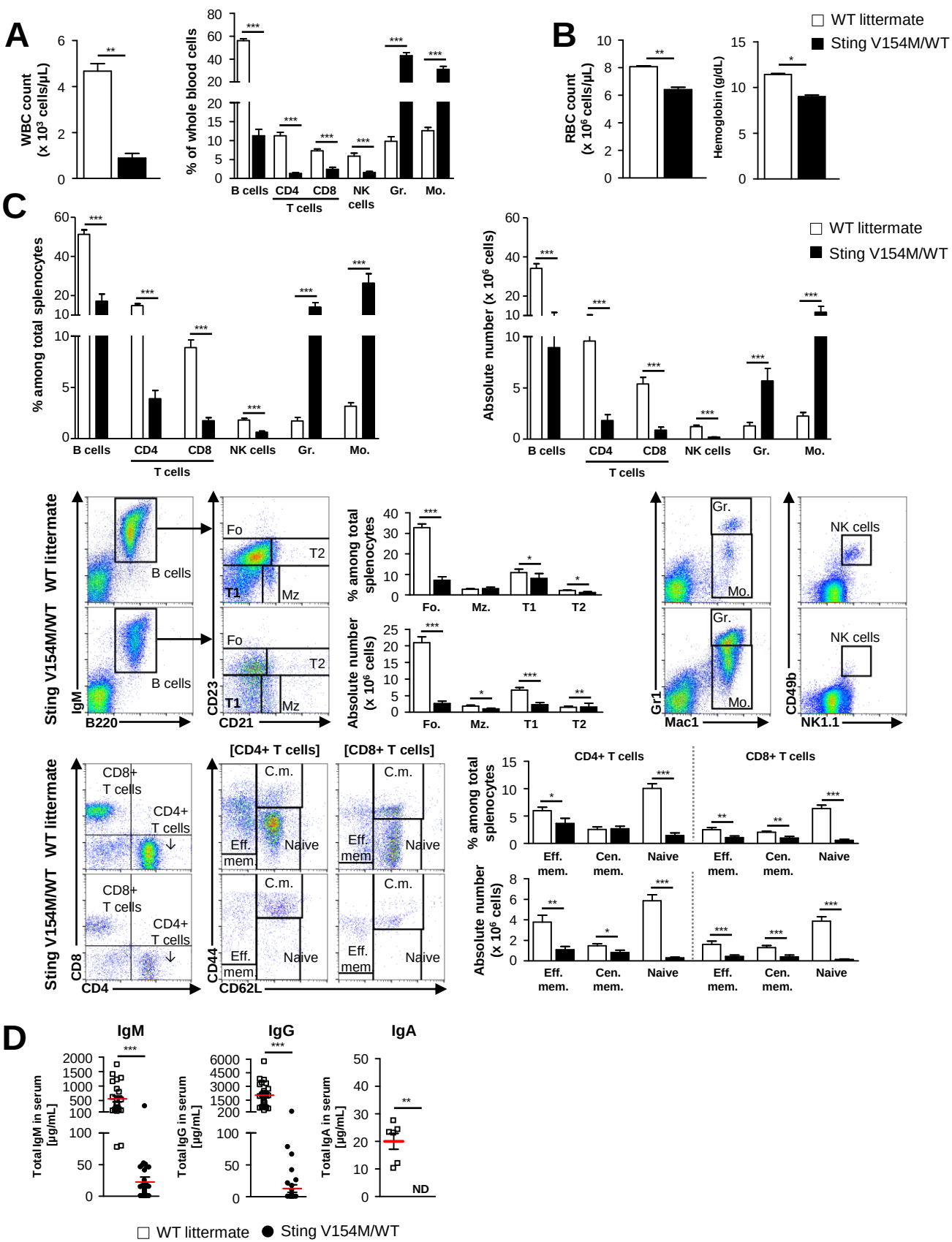
A
WBC count (x 10³ cells/µL)
% of whole blood cells
B cells
CD4
CD8
T cells
NK cells
Gr.
Mo.
B
WT littermate
Sting V154M/WT
RBC count (x 10⁶ cells/µL)
Hemoglobin (g/dL)
C
% among total splenocytes
Absolute number (x 10⁶ cells)
Sting V154M/WT
WT littermate
IgM
B220
CD23
CD21
Fo
T1
T2
Mz
Gr1
Mac1
CD49b
NK1.1
NK cells
CD8
CD4
CD44
CD62L
CD8+ T cells
CD4+ T cells
[CD4+ T cells]
[CD8+ T cells]
C.m.
Eff. mem.
Naive
Cen. mem.
D
IgM
IgG
IgA
Total IgM in serum [µg/mL]
Total IgG in serum [µg/mL]
Total IgA in serum [µg/mL]
ND
WT littermate
Sting V154M/WT

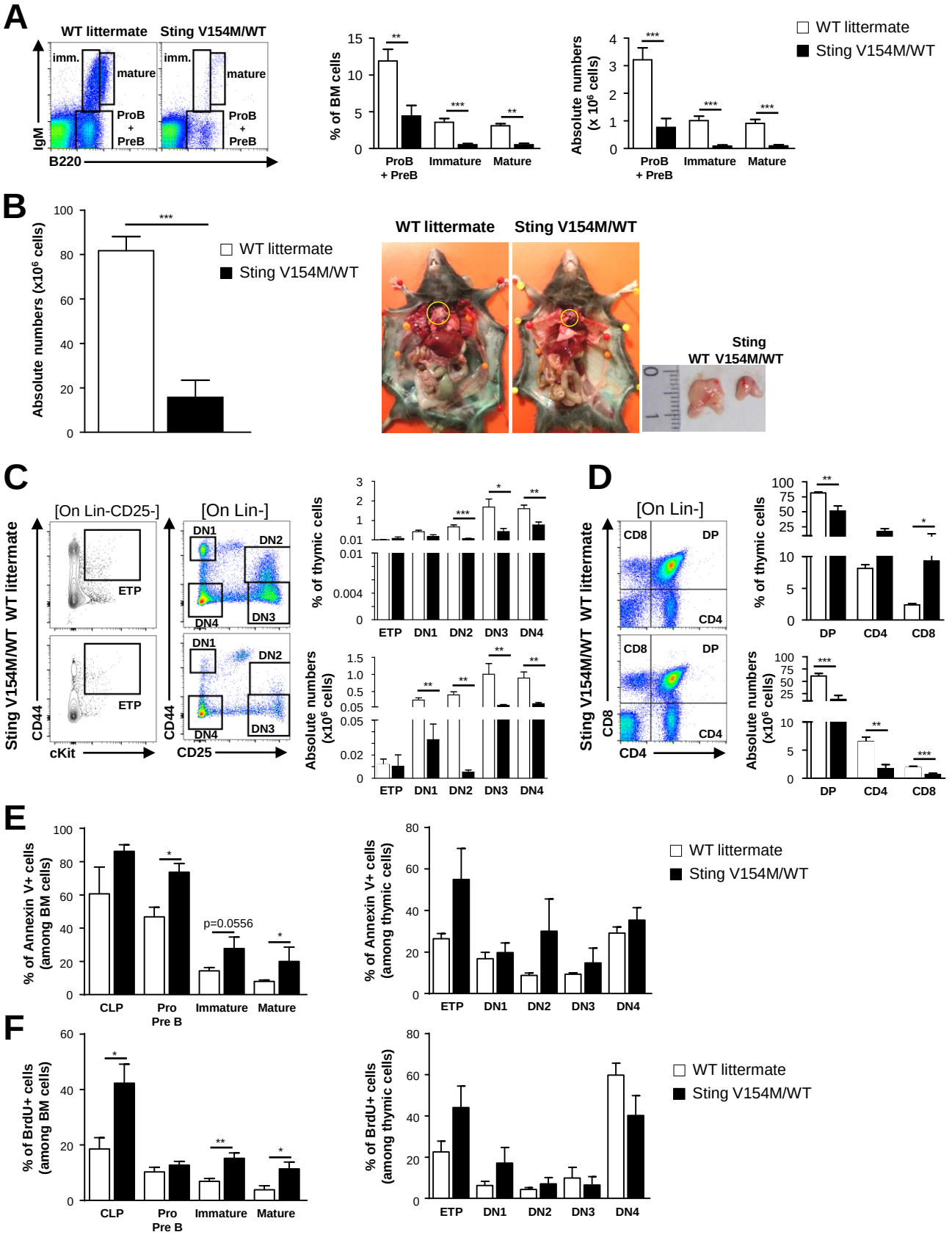
A
WT littermate
Sting V154M/WT
imm.
mature
ProB + PreB
IgM
B220
% of BM cells
Absolute numbers (x 10^6 cells)
ProB + PreB
Immature
Mature
WT littermate
Sting V154M/WT
B
Absolute numbers (x10^6 cells)
WT littermate
Sting V154M/WT
Sting
WT V154M/WT
C
[On Lin-CD25-]
[On Lin-]
Sting V154M/WT WT littermate
CD44
cKit
CD25
ETP
DN1
DN2
DN3
DN4
% of thymic cells
Absolute numbers (x10^6 cells)
D
[On Lin-]
CD8
CD4
DP
Sting V154M/WT WT littermate
% of thymic cells
Absolute numbers (x10^6 cells)
E
% of Annexin V+ cells (among BM cells)
p=0.0556
CLP
Pro Pre B
Immature
Mature
% of Annexin V+ cells (among thymic cells)
ETP
DN1
DN2
DN3
DN4
WT littermate
Sting V154M/WT
F
% of BrdU+ cells (among BM cells)
% of BrdU+ cells (among thymic cells)

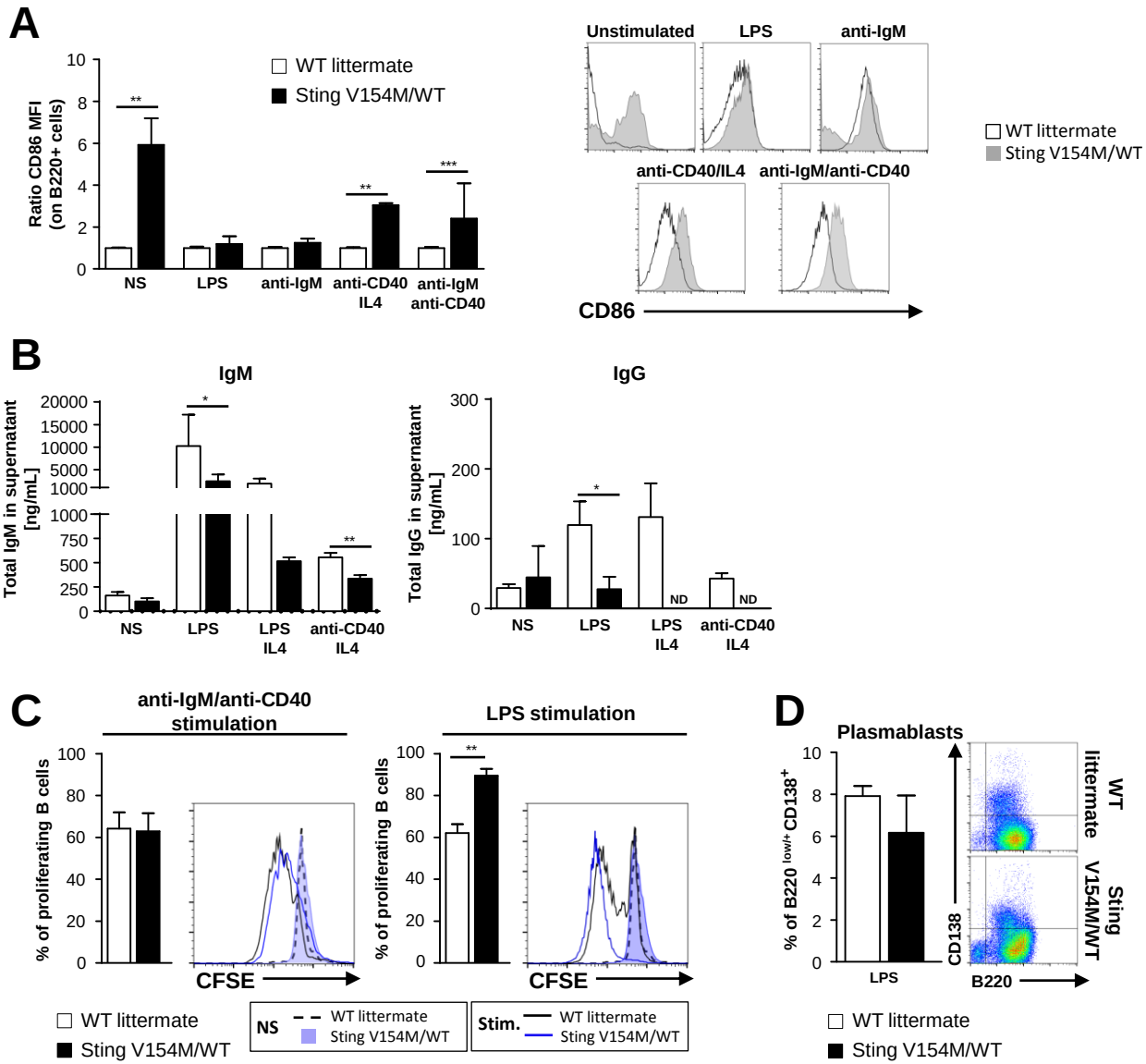
A
Ratio CD86 MFI (on B220+ cells)
WT littermate
Sting V154M/WT
NS
LPS
anti-IgM
anti-CD40 IL4
anti-IgM anti-CD40
Unstimulated
LPS
anti-IgM
anti-CD40/IL4
anti-IgM/anti-CD40
CD86
B
IgM
IgG
Total IgM in supernatant [ng/mL]
Total IgG in supernatant [ng/mL]
ND
LPS IL4
C
anti-IgM/anti-CD40 stimulation
LPS stimulation
% of proliferating B cells
CFSE
NS
Stim.
D
Plasmablasts
% of B220 low/+ CD138+
CD138
B220
WT littermate
Sting V154M/WT
E
% of Annexin V+ B cells

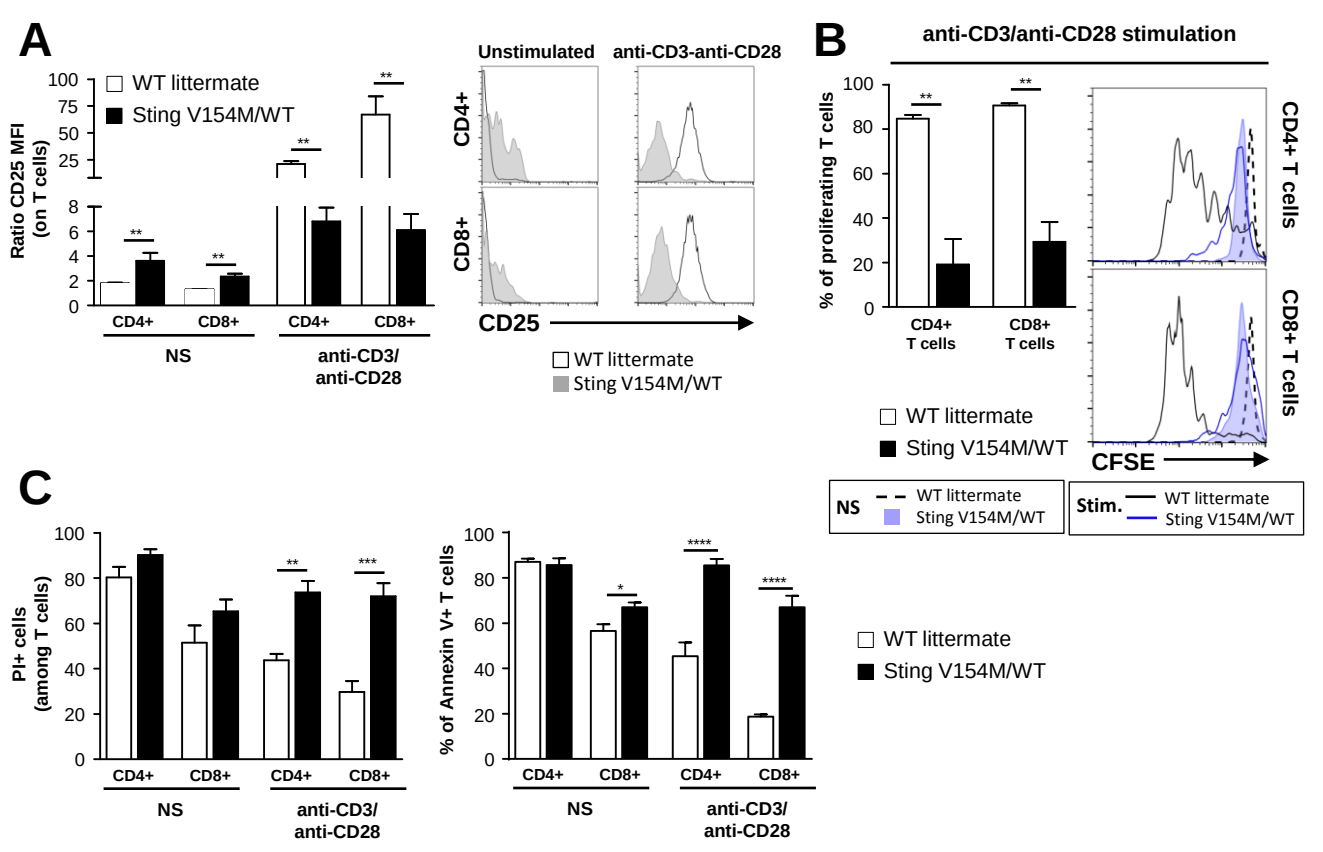
A
WT littermate
Sting V154M/WT
Ratio CD25 MFI (on T cells)
CD4+
CD8+
NS
anti-CD3/ anti-CD28
Unstimulated
anti-CD3-anti-CD28
CD25
B
anti-CD3/anti-CD28 stimulation
% of proliferating T cells
CD4+ T cells
CD8+ T cells
CFSE
NS
Stim.
C
PI+ cells (among T cells)
% of Annexin V+ T cells

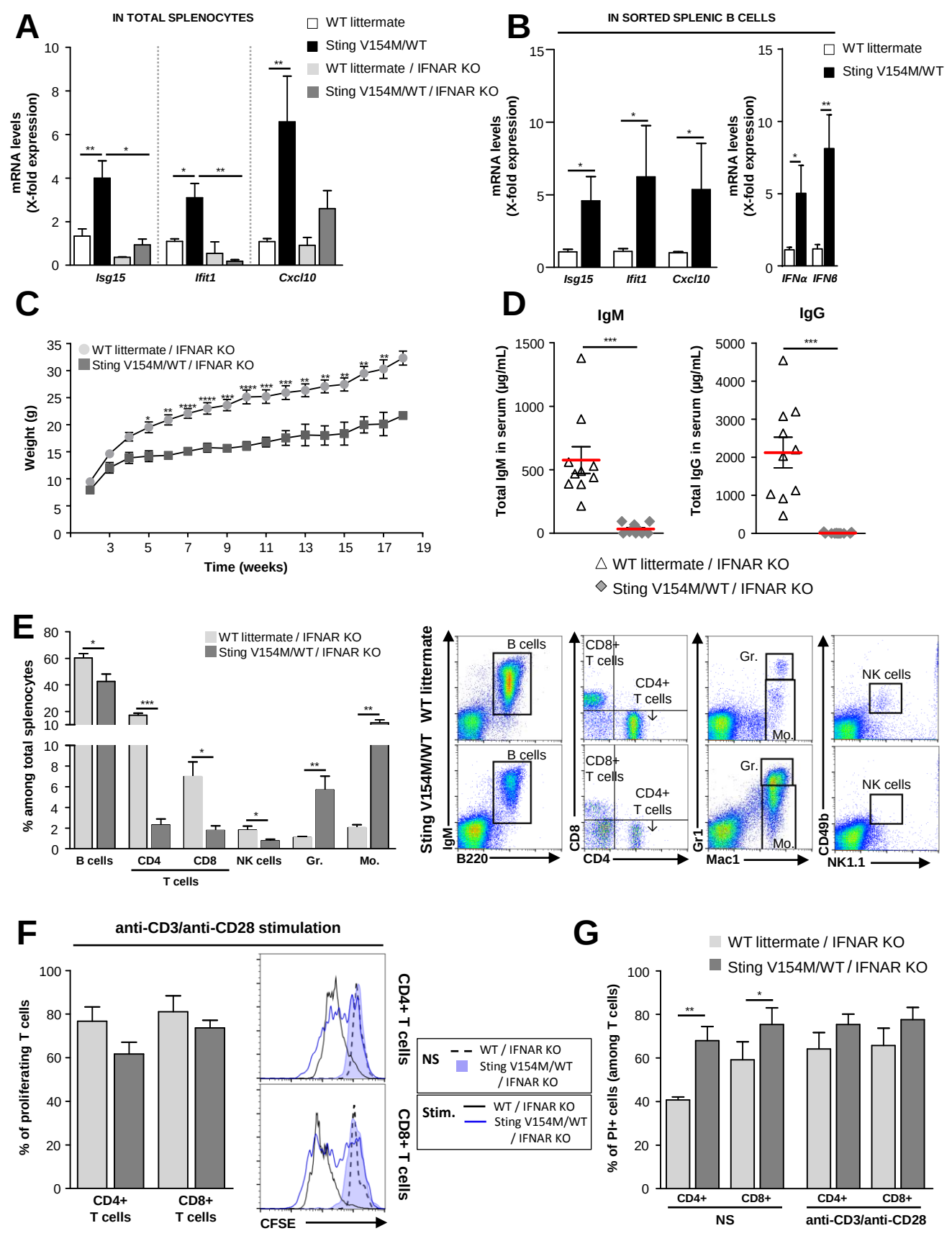
A
IN TOTAL SPLENOCYTES
WT littermate
Sting V154M/WT
WT littermate / IFNAR KO
Sting V154M/WT / IFNAR KO
mRNA levels (X-fold expression)
Isg15
Ifit1
Cxcl10
B
IN SORTED SPLENIC B CELLS
WT littermate
Sting V154M/WT
mRNA levels (X-fold expression)
Isg15
Ifit1
Cxcl10
IFNα
IFNß
C
WT littermate / IFNAR KO
Sting V154M/WT / IFNAR KO
Weight (g)
Time (weeks)
D
IgM
IgG
Total IgM in serum (µg/mL)
Total IgG in serum (µg/mL)
WT littermate / IFNAR KO
Sting V154M/WT / IFNAR KO
E
WT littermate / IFNAR KO
Sting V154M/WT / IFNAR KO
% among total splenocytes
B cells
CD4
CD8
NK cells
Gr.
Mo.
T cells
WT littermate
Sting V154M/WT
B cells
CD8+ T cells
CD4+ T cells
Gr.
Mo.
NK cells
IgM
B220
CD8
CD4
Gr1
Mac1
CD49b
NK1.1
F
anti-CD3/anti-CD28 stimulation
% of proliferating T cells
CD4+ T cells
CD8+ T cells
CFSE
CD4+ T cells
CD8+ T cells
NS
WT / IFNAR KO
Sting V154M/WT / IFNAR KO
Stim.
WT / IFNAR KO
Sting V154M/WT / IFNAR KO
G
WT littermate / IFNAR KO
Sting V154M/WT / IFNAR KO
% of PI+ cells (among T cells)
CD4+
CD8+
NS
CD4+
CD8+
anti-CD3/anti-CD28